Representation of weather situations above a certain geographical point and for the whole hemisphere by empirical orthogonal functions.

H. Fechner

Kiel

1. *Introduction*

Two different examples are given for representing weather situations by empirical orthogonal functions. First the weather situations at a certain geographical point are represented by the example of the ocean weather ship C. The second example deals with the geopotential height of the 500 mb pressure level in the Northern Hemisphere. In both examples the annual range is calculated and treated separately. In preceding examples the annual range has not been calculated separately. The special point of the first example is the use of different weights for the different physical parameters, thus the value of all parameters gets the physical dimension of the square root of energy. The special point of the second example is the representation of all the geographical fields by series of surface spherical harmonics also when computing the empirical orthogonal functions.

2. *Classification of weather situations at the ocean weather ship C by vertical empirical orthogonal functions*

In a preceding investigation at our Institute (ERDMANN (1973), ERDMANN and FECHNER (1974)), the empirical time independent orthogonal functions of a set of data, including geopotential height, temperature and moisture, were computed at the radiosonde station Erlangen/Stuttgart between 900 mb and 400 mb. The investigation also considered the seasonal influence

We wanted to separate the mean annual range of all parameters from the synoptic disturbances. Only the last should be developed into empirical orthogonal functions. So we need the annual range for each day of the year. In order to get a continuous function of time with the period of a year, each parameter was represented by a Fourier series with the period of one year. Its coefficients were computed from monthly mean values. Therefore, we could only compute terms up to wave number 5. Then the series has 11 terms. We got a function with values for each day of the year without any discontinuities. This function is the annual range. We computed it for each parameter, thus we get 63 functions. In Fig. 2 you see the annual range of the 500 mb geopotential height, and in Fig. 3 the same for the temperature.

The specific humidity decreases very rapidly with decreasing pressure. Therefore the specific humidity is presented for the 1000 mb level in Fig. 4. For the wind velocity components there are contour lines presented in a cross section of time and pressure (Fig. 5 and 6). For these two figures the parameters measured originally with a 50 mb resolution are used and not their means over three levels, which were used in other computations.

In our other calculations only deviations of the measured parameters from these annual ranges are used.

Before we can use the different physical parameters for the computation of the coefficients, they must get the same physical dimension. For this dimension we used the square root

of the energy per unit mass. Then eigenvalues get the physical dimension of energy per unit mass. This conception of the weights for the different physical parameters is based on the idea that the physical relationship between them will be caused by energy transfer.

For the wind velocity components no special weight is necessary. But for the geopotential height Φ and the temperature T we have to look for a connection between the square of the geopotential height or the square of the temperature on one side and the energy on the other side. Such a connection can be found in the theory of available potential energy (LORENZ, Tellus 7, 157-167, 1955). For the stability γ we used a time independent, but pressure p dependent function for this area. We got it from the paper of P. SPETH: Die verfügbare potentielle Energie und der Transfer zwischen zonaler und turbulenter verfügbarer potentieller Energie der Hamburger Sturmflut-wetterlage vom Februar 1962. Beitr. Phys. Atmosph. 45, 121-147, 1972. The humidity q was connected with the temperature T by the latent heat L. So the following formulas were used for the geopotential height:

$$f_g = \sqrt{\frac{R}{C_v}\,\frac{C_p}{C_v}}\;\sqrt{\gamma}\,(\Phi-\overline{\Phi}),$$

for the temperature

$$f_T = \sqrt{\frac{C_p}{C_v}}\;\sqrt{\gamma}\;(T-\overline{T}),$$

and for the humidity

$$f_h = \frac{L}{C_p} \sqrt{\frac{\gamma}{2}} \, (q-\bar{q})$$

with

$$\gamma = \frac{R}{p} \frac{\tilde{\theta}}{\tilde{T}} \left(- \frac{d\tilde{\theta}}{dp}\right)^{-1}.$$

C_p and C_v are the specific heats at constant pressure and constant volume respectively, R is the gas constant of air, and $\theta = T(\frac{1000 \text{ mb}}{p})^{R/C_p}$ the potential temperature, $\bar{X}$ means the value of the annual variation of X, and $\tilde{X}$ means the average of X over the total period. The weighted parameters f_x are also functions of time: f_{xt}, they were used for the calculation of the covariance matrix, the eigenvectors and their eigenvalues. From the f_{xt} we got the covariance matrix $A = (a_{xy})$ with

$$a_{xy} = \frac{1}{t_2} \sum_{t=1}^{t_2} f_{xt} \cdot f_{yt} \; ;$$

and from this the eigenvalues w_k^2 and the eigenvectors g_{xk} are calculated by the eigenvalue equation

$$\sum_{y=1}^{63} a_{xy} g_{yk} = w_k^2 \, g_{xk} \qquad (x=1,\ldots,63)$$

and the special normalisation $\sum_{x=1}^{63} g_{xk}^2 = w_k^2$.

The g_{xk} were computed by the iteration algorithm of JACOBI, see SPERNER (1957) and GREENSTAD (1967).

In order to prove the confidence or stability of the covariance matrix, or what is the same, of the eigenvectors and eigenvalues, the number of soundings used t_2 was reduced from 13,000 to 900. Then only a slight difference in the wind components of the eigenvectors g_{xk} arose. All eigenvalues w_k^2 and all the other values of g_{xk} remained nearly unchanged.

At a first result we get the eigenvalues; their sequence is shown in Fig. 7. The first eigenvalue has a magnitude of 1.503 J/g, that is three times the second eigenvalue which is 0.49 J/g.

The mean-square error of the partial series is given by the formula

$$F_n^2 = \sum_{k=n+1}^{63} w_k^2 .$$

$F_o^2 = \sum_{k=1}^{63} w_k^2$ is the total variance. In Fig. 8 you can see the relative mean-square error. When using only five terms the partial series has a mean-square error of 22 %. The vertical and the physical structure of the coefficients g_{xk} for k=1,2,3,4,5 is given on the Fig. 9 up to 18. In the figures with odd numbers the values of the eigenvectors are presented with the weight in the common physical dimension of the square root of Joule per gramme. On the figures with the even number the values of the eigenvectors are presented without weights in their real physical dimension. The relation between different physical

values in both presentation modes is identical only for the 500 mb level.

In the first coefficient, Fig. 9 and 10, the temperature has its minimum of -4.95K nearly at the 500 mb level, it is zero at 280 mb, which is the level of the mean tropopause, and its maximum value of +4.07K is situated at 200 mb.
The geopotential height has its minimum value of -185 gpm at the 300 mb level. The humidity has its minimum of 0.7 g/kg at 900 mb, and it has a positive correlation with the temperature. Also the v-component has a positive correlation with the temperature, that means wind from N = negative v-value is correlated with cold air masses and vice versa. So one could say, the first coefficient represents the (cold) air mass.

In the second coefficient, Fig. 11 and 12, the wind is dominated by negative values for v(=wind from N) and positive values for u (= more wind from W), both with an approximate absolute value of 10 m/sec. The second coefficient represents cold continental air from NNW.

The third coefficient, Fig. 13 and 14, characterizes nearly only the wind (less from W, a little more from N).

The fourth coefficient, figures 15 and 16, characterizes the geopotential height and the wind, but more the v-component, wind from south in the middle of the atmosphere. In the last important coefficient, the fifth mode which is presented in figures 17 and 18, the most important property is the

stability of the air mass, that means: cold air near the ground and warm air in the middle of the atmosphere.

All other coefficients represent only 16% of the total variance, thus they can be neglected. The theory of the empirical orthogonal functions shows that each parameter f_x can be represented at each time t by the sum of the time independent coefficients multiplied with the corresponding time dependent coefficients c_{kt}:

$$f_{xt} = \sum_{k=1}^{63} c_{kt} \cdot g_{xk} .$$

These coefficients c_{kt} are uncorrelated; in formula

$$\frac{1}{t_2} \sum_{t=1}^{t_2} c_{kt} c_{jt} = \begin{cases} 1 & \text{for } k=j \\ 0 & \text{for } k \neq j \end{cases} .$$

In Fig. 19 the first five coefficients for the selected period are shown. They were compared with the weather maps of the corresponding time and the above described properties of the different modes described above could be verified.

3. *Climatology of the Northern Hemisphere by using coefficients of the 500 mb topography in the wave number domain*

In a preceding investigation of FECHNER (1974) and FECHNER (1975) the empirical orthogonal functions of the geopotential height of the 500 mb level of the Northern Hemisphere have been calculated for the three winter months of December, January and February. In contrast to an analogous investigation of

CRADDOCK and FLOOD (1969) my calculations based on the coefficients of surface spherical harmonics and not on grid-point values. JECKSTRÖM (1977) used those coefficients and their time dependent coefficients for an optimal and objective climatology by meteorological interpretation. In order to obtain a climatology of the entire year a new computation was made using all months (FECHNER (1978)). The data used were obtained from the German Weather Service for the period of 1966 until 1974. They are given on an octal grid with 2372 points, see Fig. 20, which covers nearly the whole Northern Hemisphere each 12 hours. These data fields have been transferred into spectral form, so that they are represented by the coefficients of surface spherical harmonics up to wave number 15 with triangular truncation. Theharmonics used are reflected at the equator. Each field is represented by 136 coefficients. The computation from grid-point representation to spectral representation was done using a least-square method. In all further computations only these coefficients of the surface spherical harmonics are used. Thus the results are in the wavenumber domain. Before beginning with the computation of the coefficients, the mean annual range of the fields was calculated by the same method as in the first example using time dependent Fourier series with a period of one year up to wave number five for the continuity in time. The mean field (time wave number zero) is given in Fig. 21. The energy per area,or the squares of the amplitudes for the other waves of the annual range, that is the variance of them, has the following values:

Time wave number per year	variance in $(gpm)^2$
1	8262
2	237
3	52
4	36
5	22

Sum of all waves = variance of the annual range 8608 $(gpm)^2$.

In the subsequent calculation only the deviation of the geopotential fields from the annual range for each half day was used. The calculation of the eigenvalues and of the empirical orthogonal functions (eofs) will be performed by the same method as in the first example, if the vector parameter x varies over all 136 surface spherical harmonic wave modes. Each geopotential field $\Phi_t(\phi,\lambda)$ can be represented by a series of eofs $g_k(\phi,\lambda)$

$$\Phi_t(\phi,\lambda) = \overline{\Phi}(t,\phi,\lambda) + \sum_{k=1}^{136} c_{kt}\, g_k(\phi,\lambda)$$

where the eofs $g_k(\phi,\lambda)$ for $k = 1,\ldots,136$ are represented by the coeficients g_{xk} of surface spherical harmonics $Y_k(\phi,\lambda) = P_n^m(\sin\phi)e^{im\lambda}$

$$g_k(\phi,\lambda) = \sum_{x=1}^{136} g_{xk} \cdot Y_k(\phi,\lambda).$$

The $P_n^m(z)$ are the associated Legendre functions with

$$\frac{1}{2}\int_{-1}^{1} \left| P_n^m(z) \right|^2 dz = 1 \ .$$

The sequence of the computed eigenvalues w_k^2 is shown in Fig. 22.

If this result is compared with the results of other investigations it must be noticed that the annual range is subtracted and its total variation is 8608 gpm^2, that is nearly 22 times of the variance of the first mode. On Fig. 23 you see the same figure in a logarithmic scale for the eigenvalues. The variances v_k^2 of the partial series are given by the sum of the eigenvalues up to the actual ordinary number k:

$$v_k^2 = \sum_{j=1}^{k} w_j^2 .$$

The increase of the variances you can see on Fig. 24. For the total variance without the annual range we got 5327 $(gpm)^2$, for the annual range we got 8608 $(gpm)^2$, thus we get for the total variance with the annual range a value of 13935 $(gpm)^2$. The variances in a logarithmic scale is given in Fig. 25.

In the next figures from 26 up to 29 the eigenfunctions of the deviations from the annual range are presented. They are numerically represented and stored by their surface spherical harmonic coefficients g_{xk}.

If the eofs are known, then the field can be developed in a series of eofs at each time. Their space independent coefficients c_{kt} vary with time t. In order to compare the coefficients c_{kt} of different modes k in absolute values,

the physical dimensionless c_{kt} are multiplied with the square root w_k of the corresponding eigenvalues. Then they have the same physical dimension as the measured parameters $\Phi(t,\phi,\lambda)$. In Fig. 30 you can see the variation of them for the first four modes for the year 1972. This variation should be computed for all years, and from those time series the energy spectra should be calculated. These results and a detailed presentation of this investigation will be given in the paper of FECHNER (1978). The same calculation could be done for the field of the air temperature and perhaps for fields of other pressure surfaces.

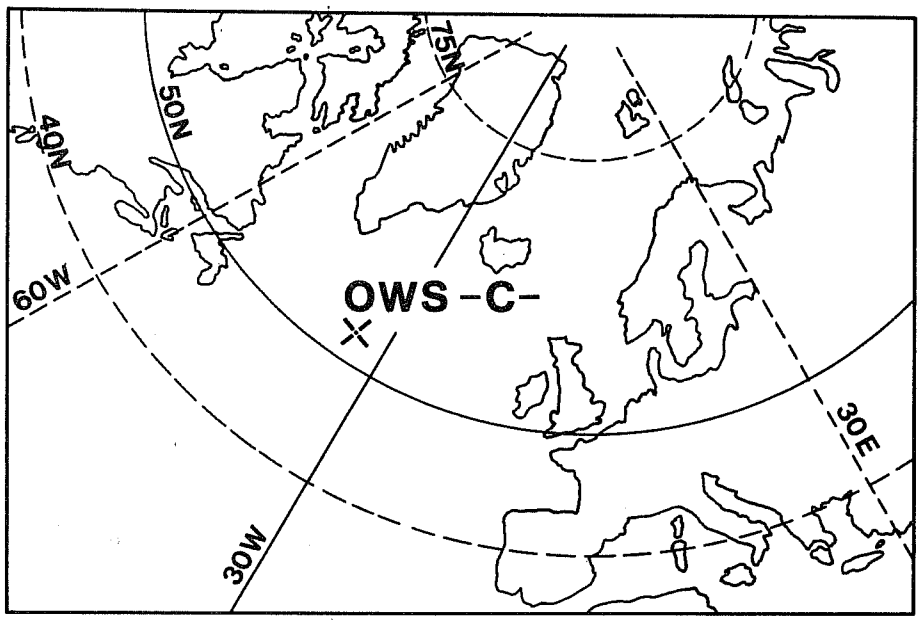

Fig. 1 Position of the ocean weather ship C.

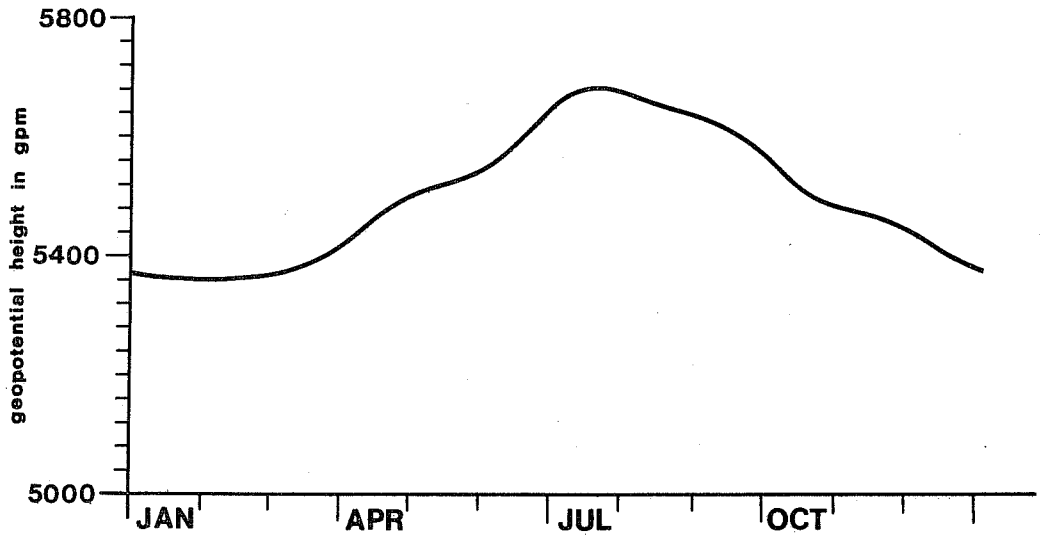

Fig. 2 The annual range of the geopotential height of the 500 mb level at the weather ship C.

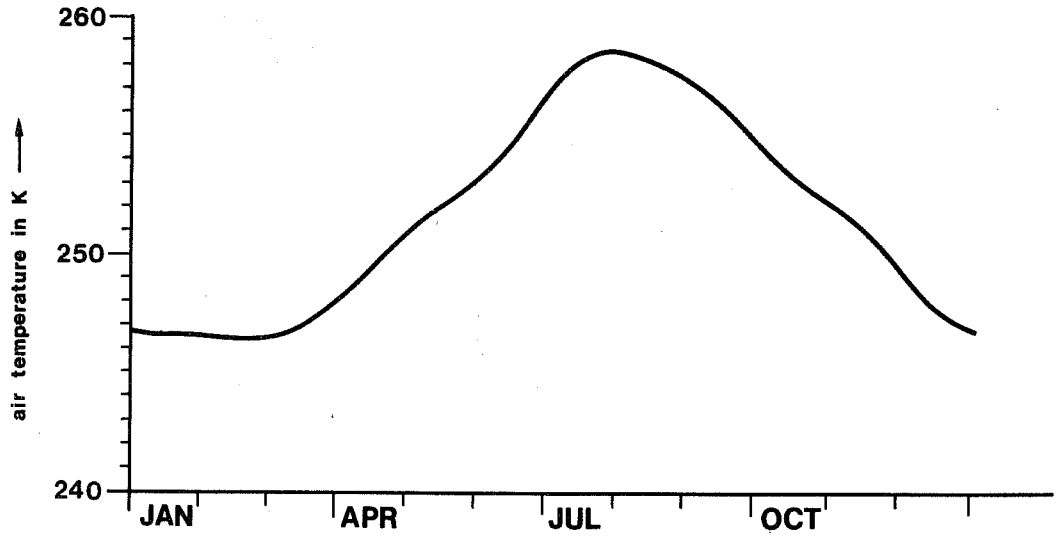

Fig. 3 The annual range of the temperature in the 500 mb level at the weather ship C.

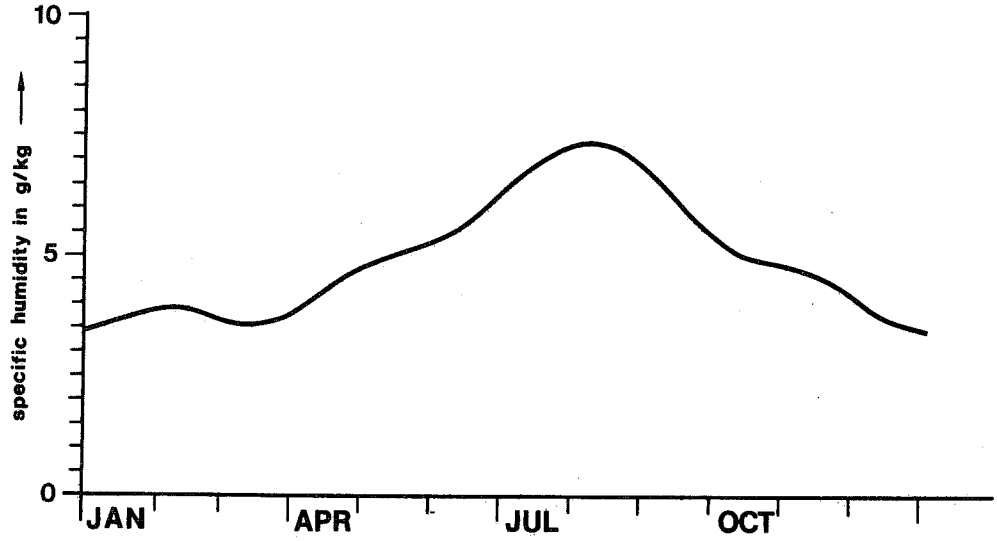

Fig. 4 The annual range of the specific humidity in the 1000 mb level at the weather ship C

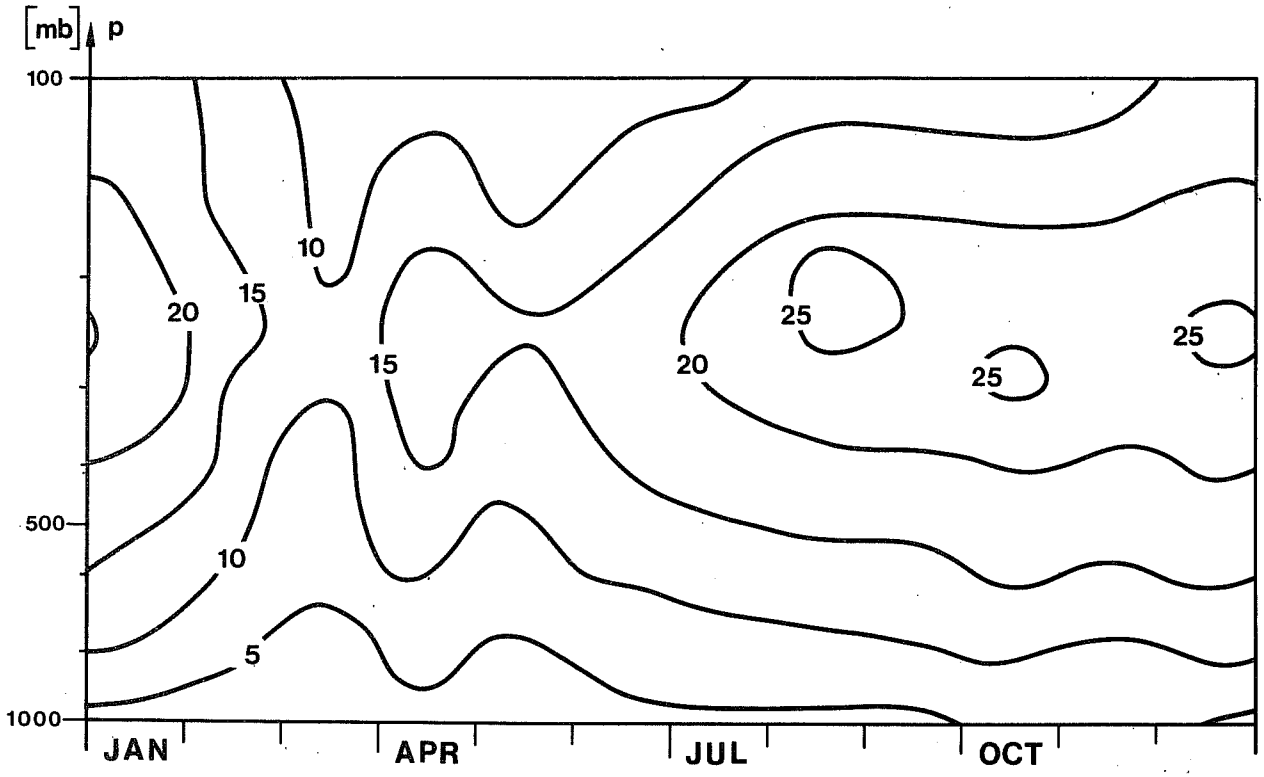

Fig. 5 The annual range of the u-component of the wind velocity in a time-pressure cross-section at the weather ship C.

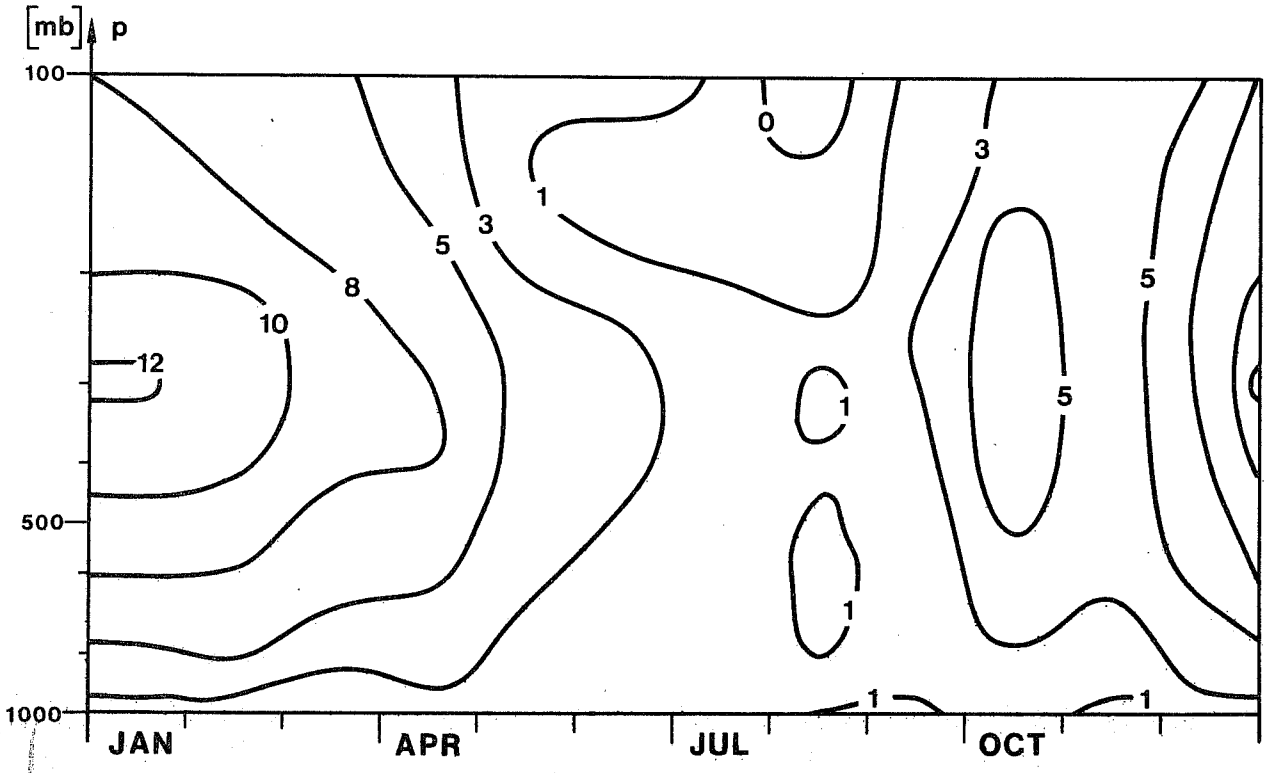

Figure 6. The annual range of the v-component of wind velocity in a time-pressure cross-section at the weather ship C.

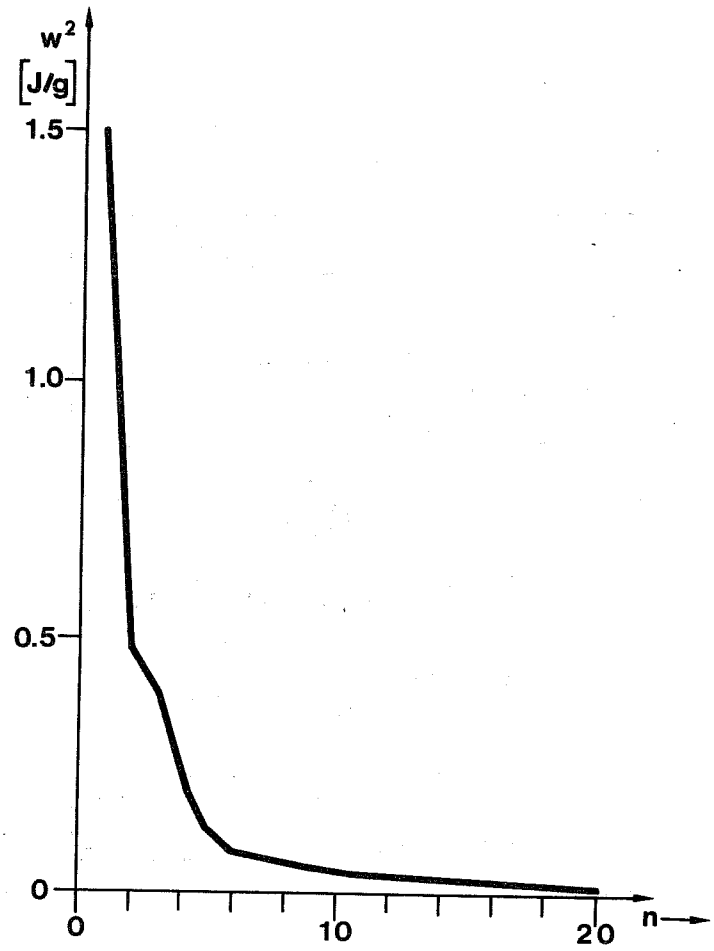

Figure 7 The eigenvalues of the covariance matrix of the deviations from the annual range of meteorological parameters at the weather ship C.

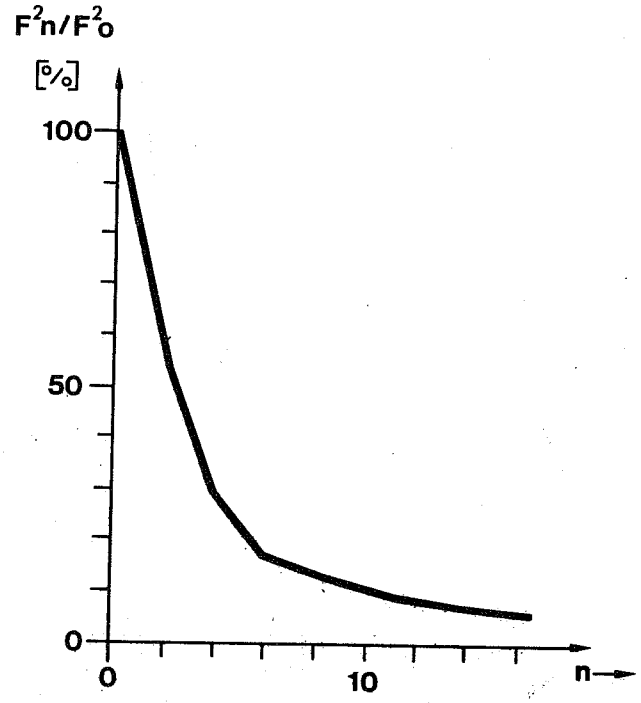

Figure 8

The mean square error of partial eof-series at the weather ship C.

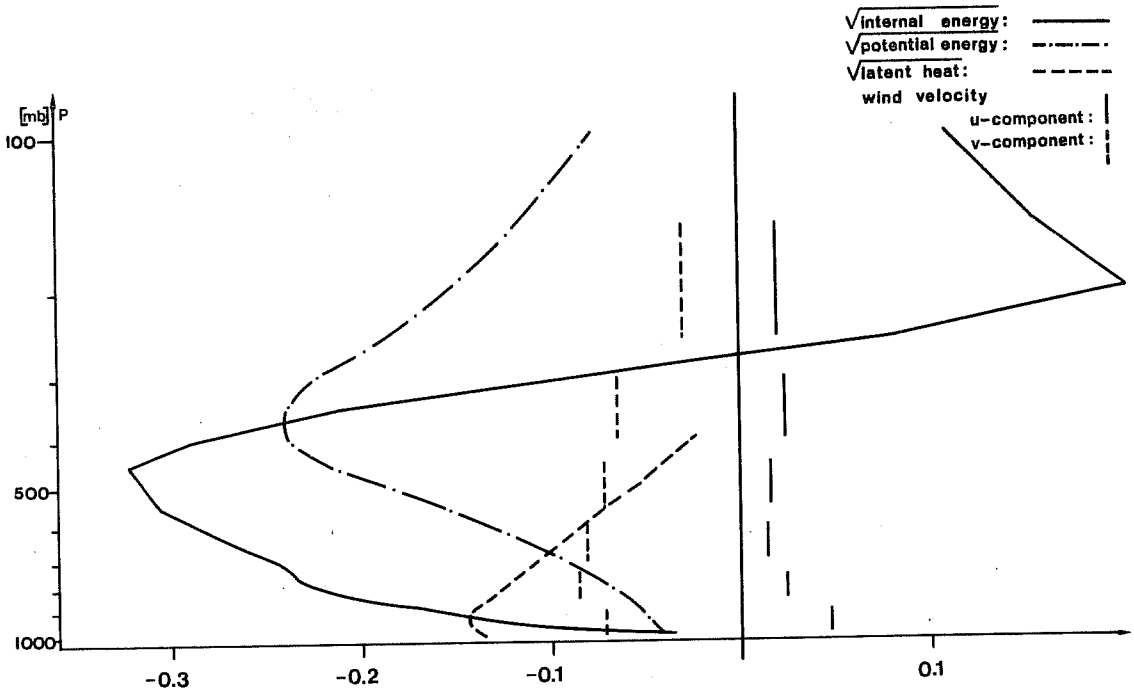

Figure 9 The first (most important) eof of meteorological values at the weather ship C, without the annual range.

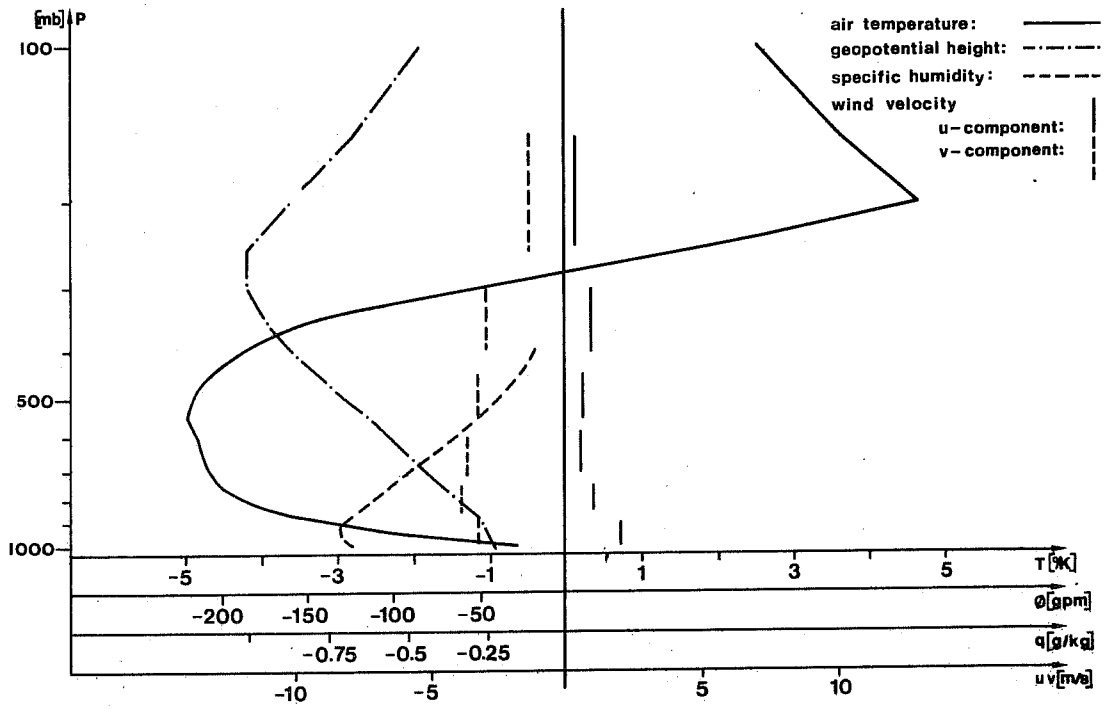

Figure 10 The first (most important) eof of meteorological values in the measured dimensions at the weather ship C, without the annual range.

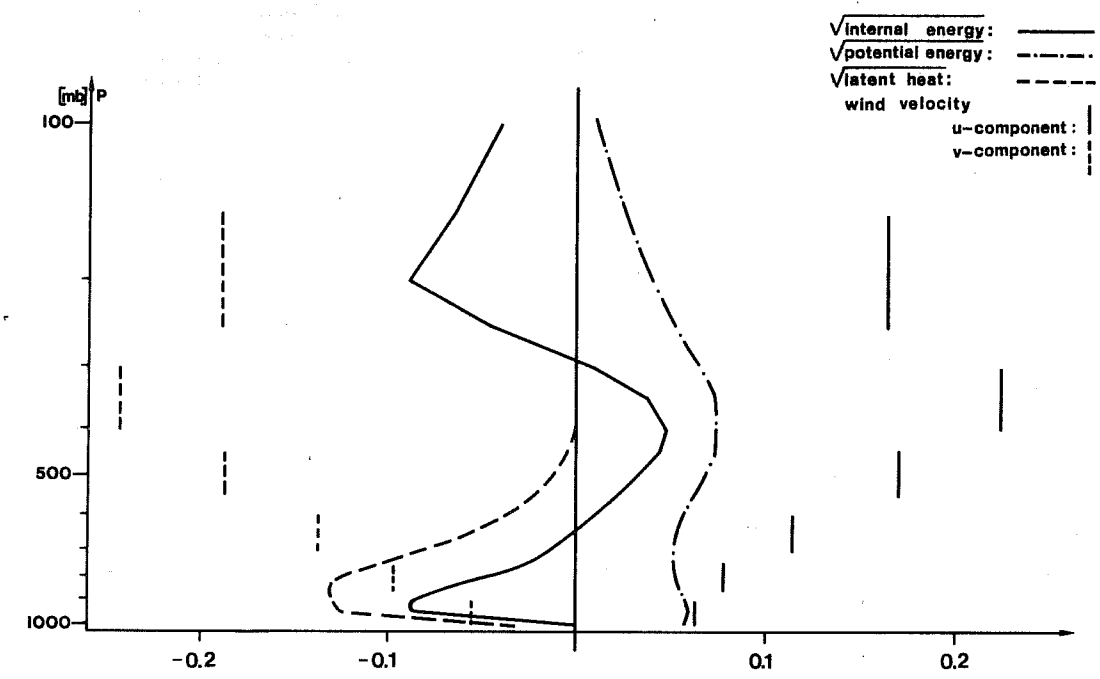

Figure 11 The second eof of meteorological eigenvalues at the weather ship C.

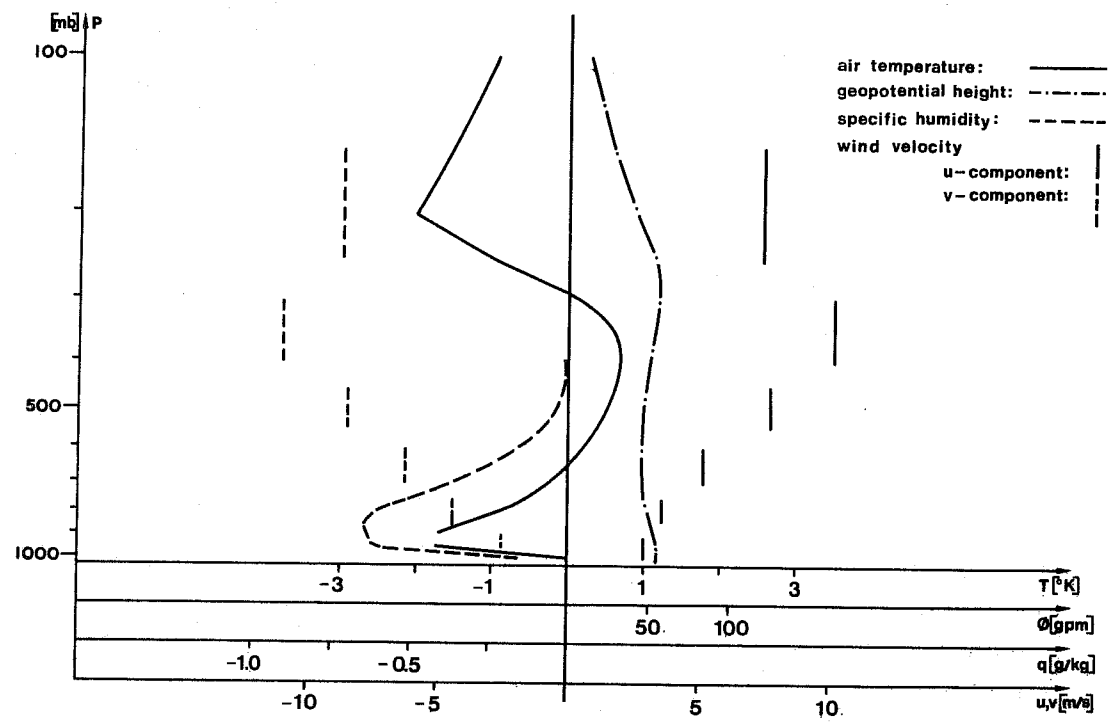

Figure 12 The second eof of meteorological values in the measured dimensions at the weather ship C.

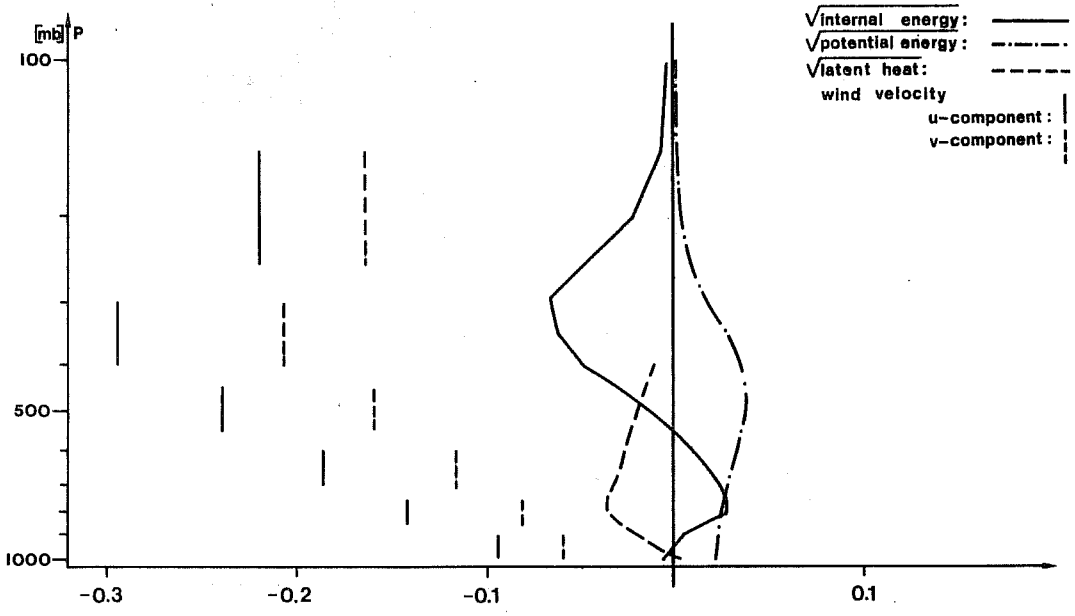

Figure 13 The third eof of meteorological values at the weather ship C.

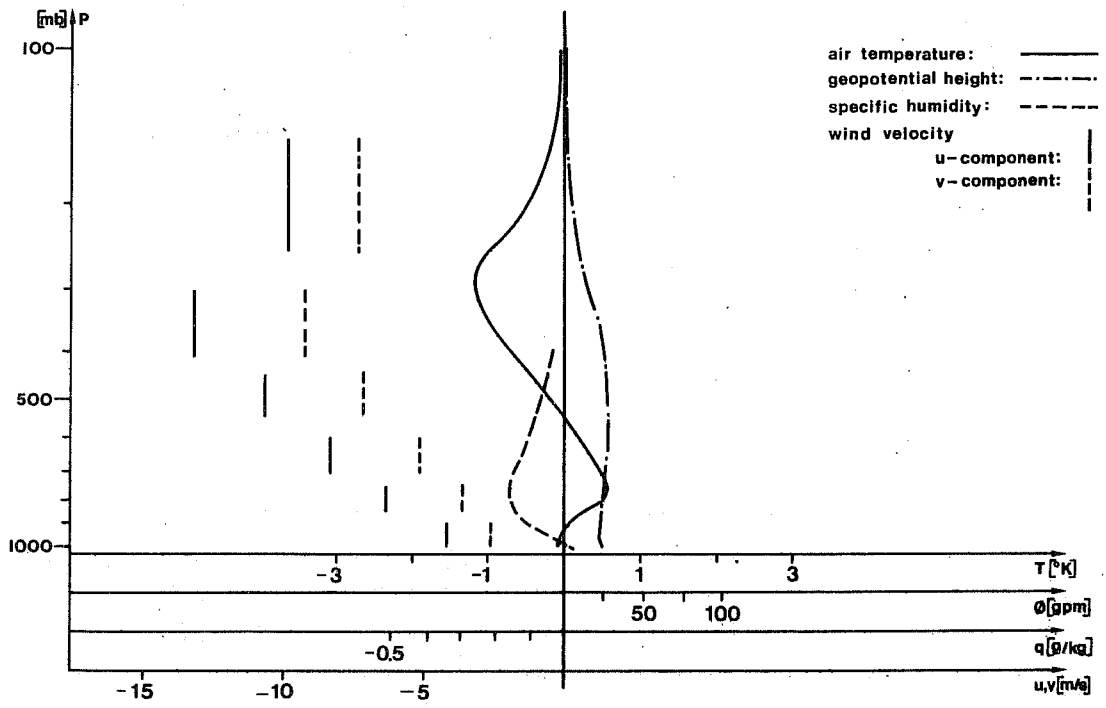

Figure 14 The third eof of meteorological values in the measured dimensions at the weather ship C.

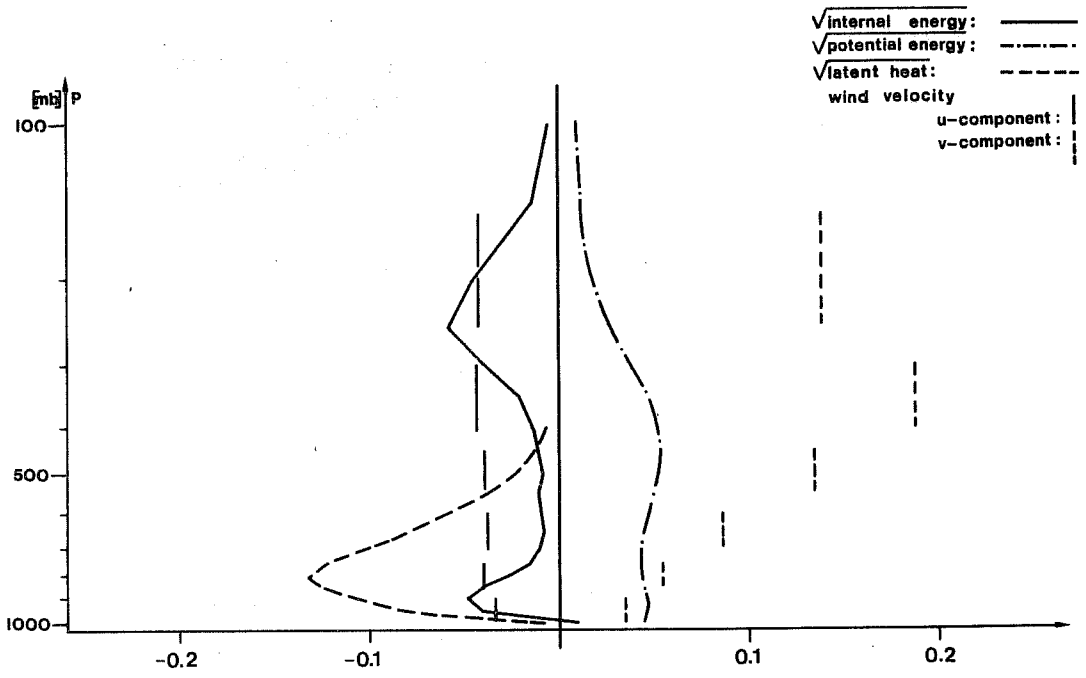

Figure 15 The fourth eof of meteorological values at the weather ship C.

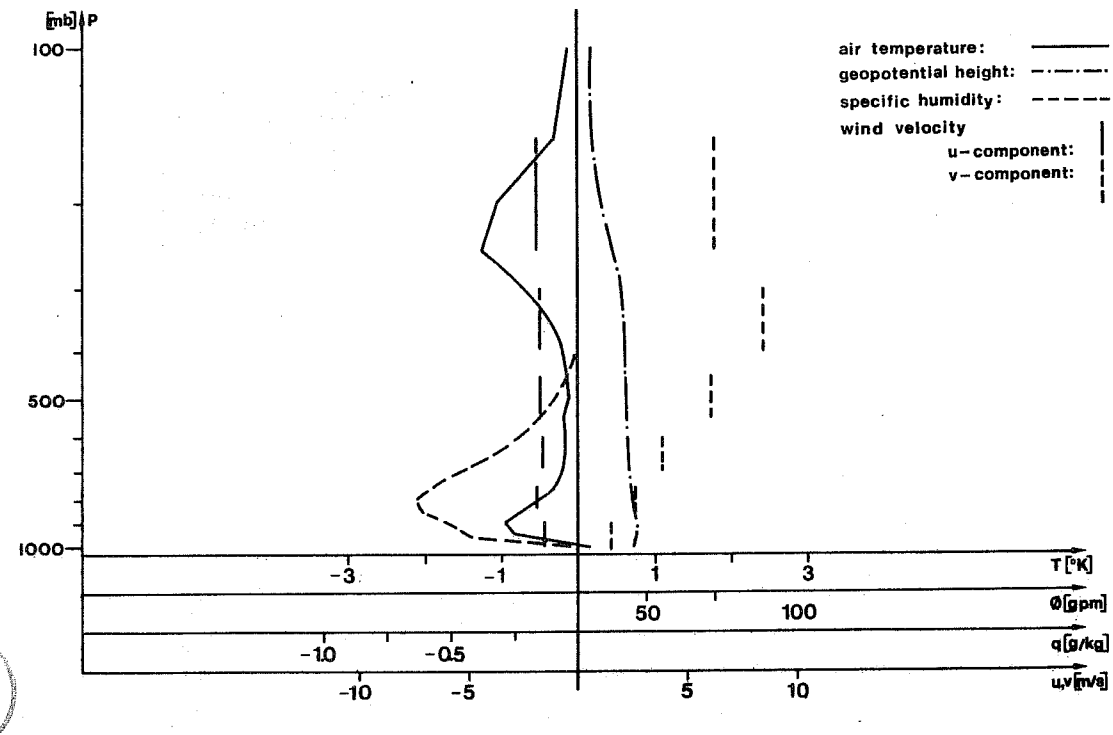

Figure 16 The fourth eof of meteorological values in the measured dimensions at the weather ship C.

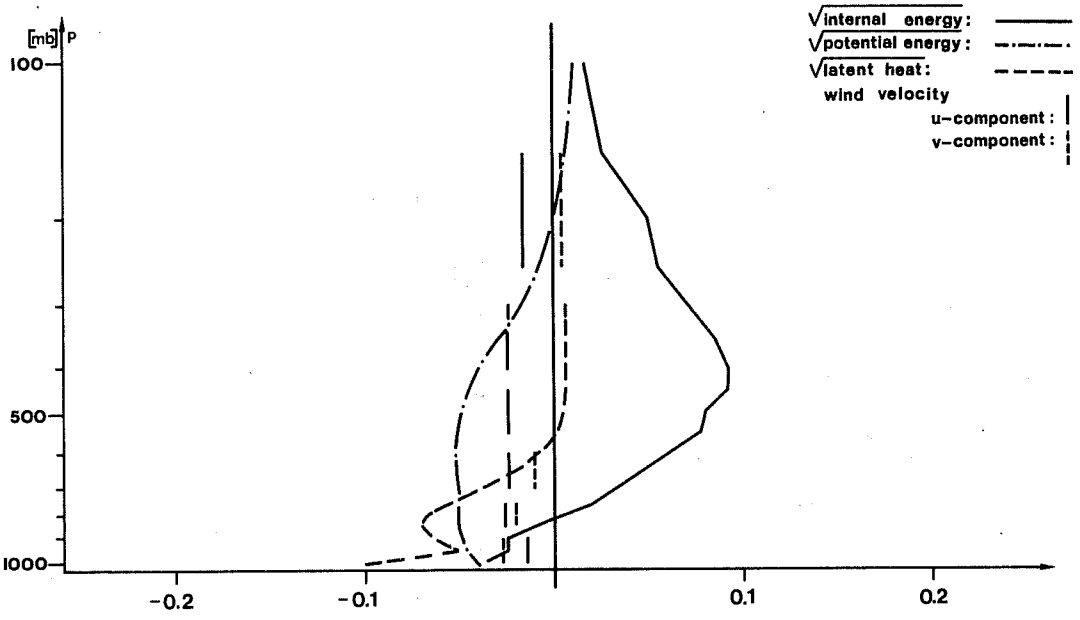

Figure 17 The fifth eof of meteorological values at weather ship C.

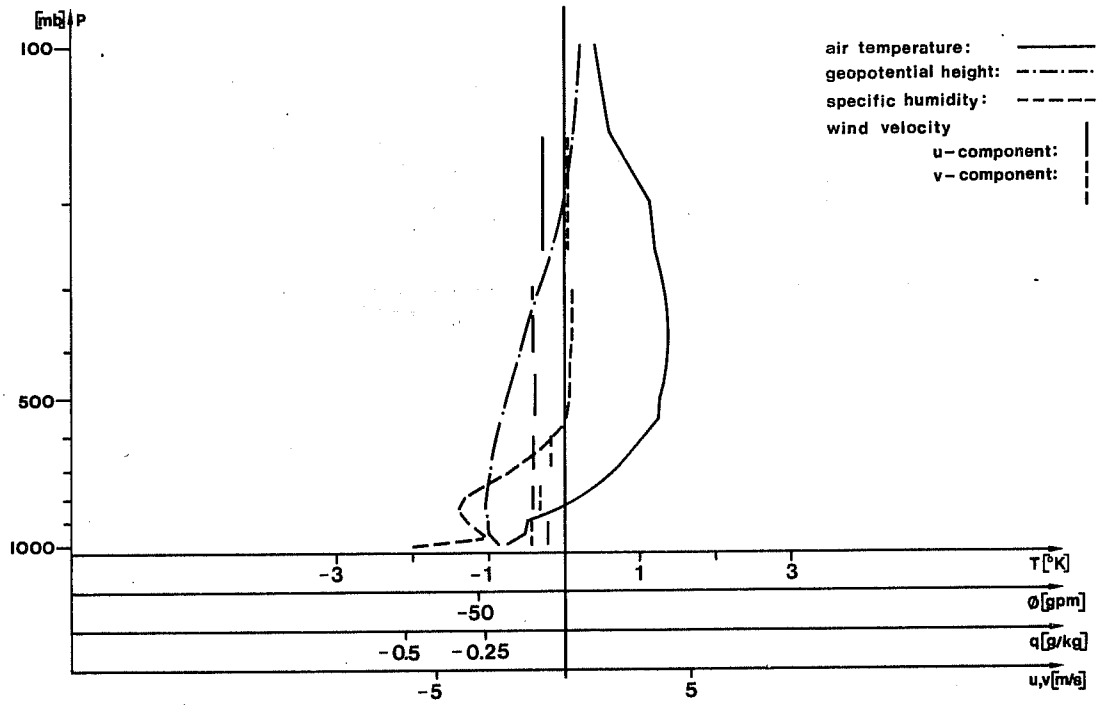

Figure 18 The fifth eof of meteorological values in the measured dimensions at the weather ship C.

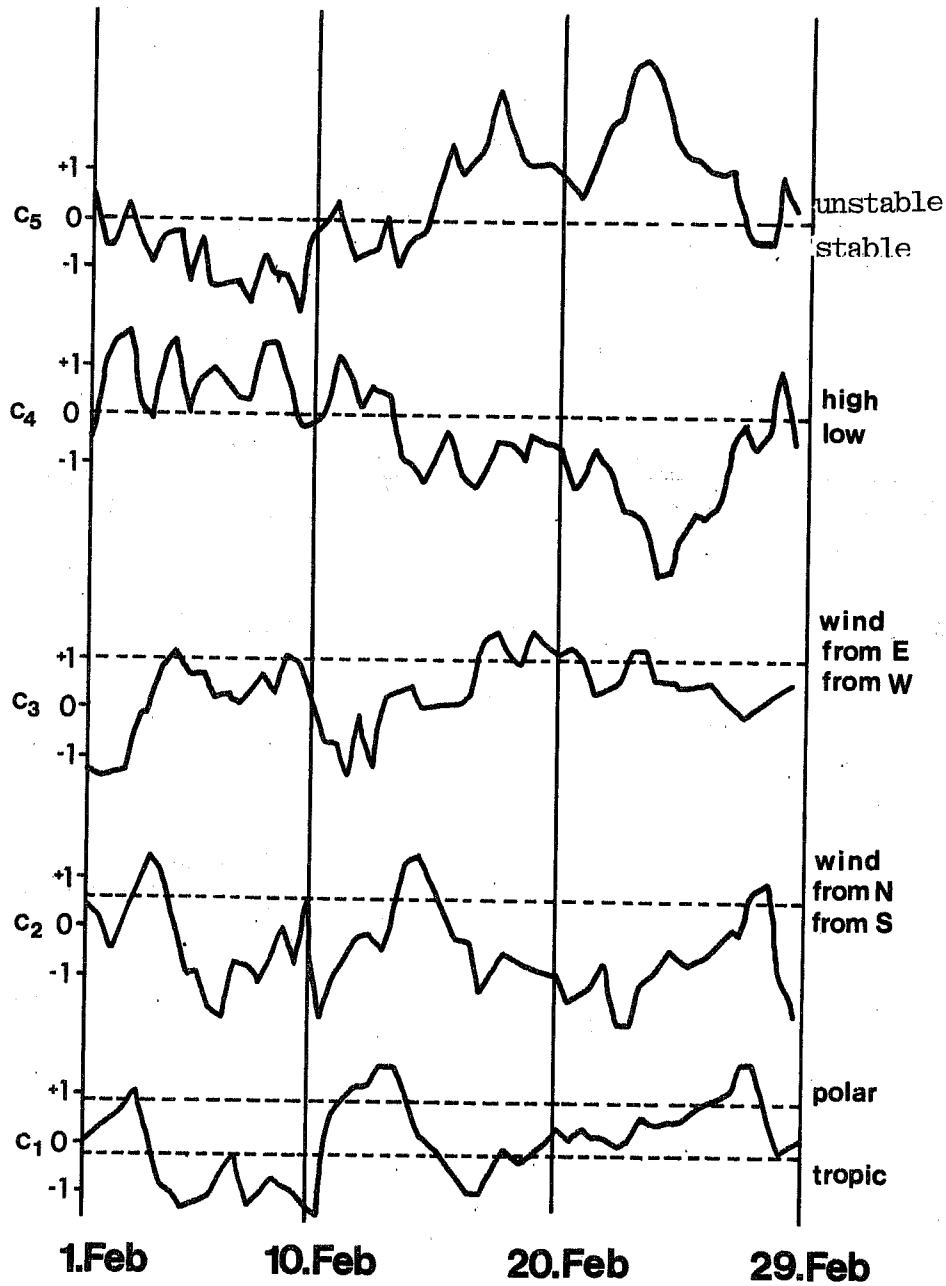

Figure 19 The five most important time dependent coefficients of the eofs at the weather ship C for a selected period of the year 1964.

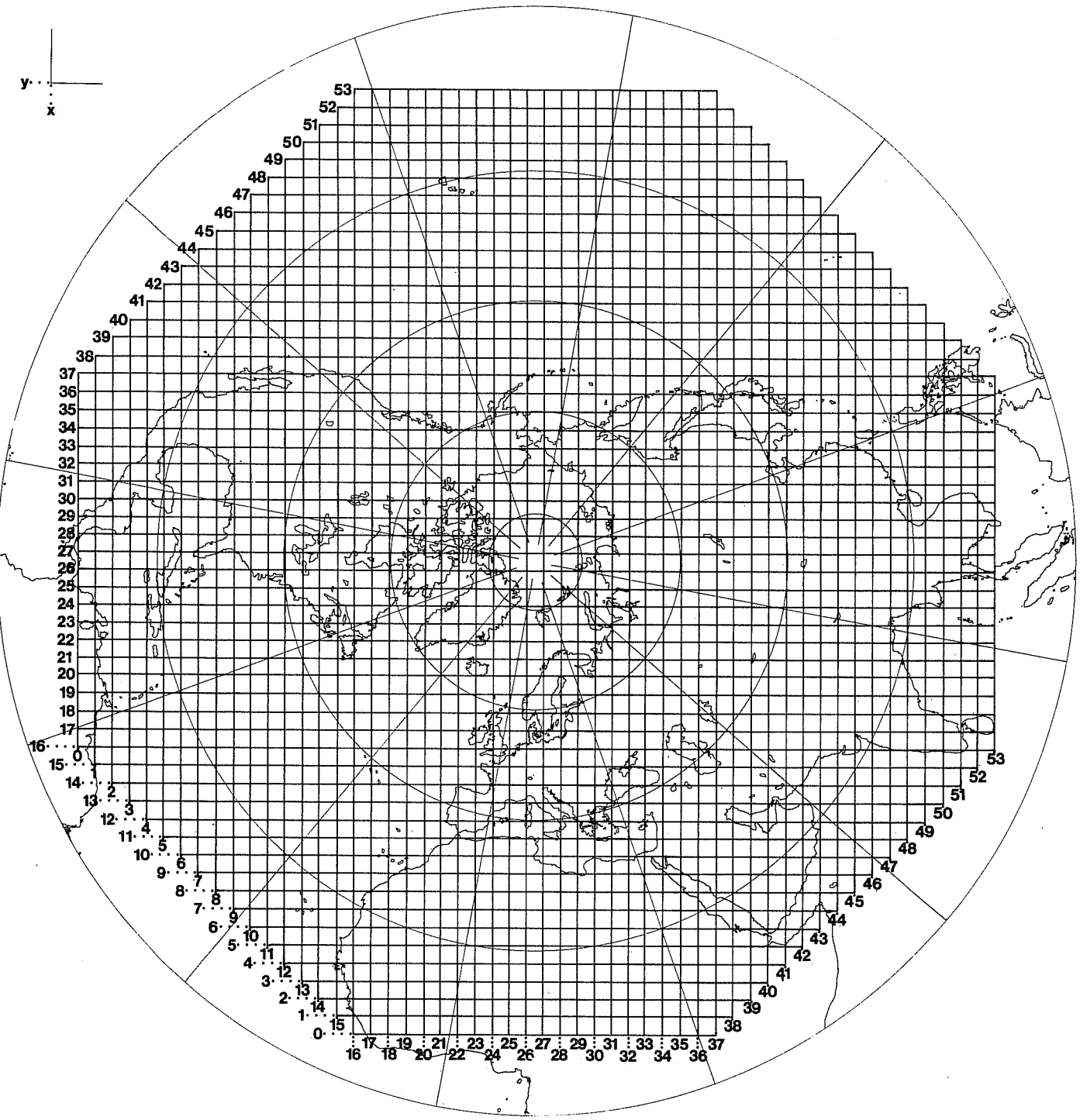

Figure 20 DWD grid on which the original values of the geopotential height of the 500 mb level are given.

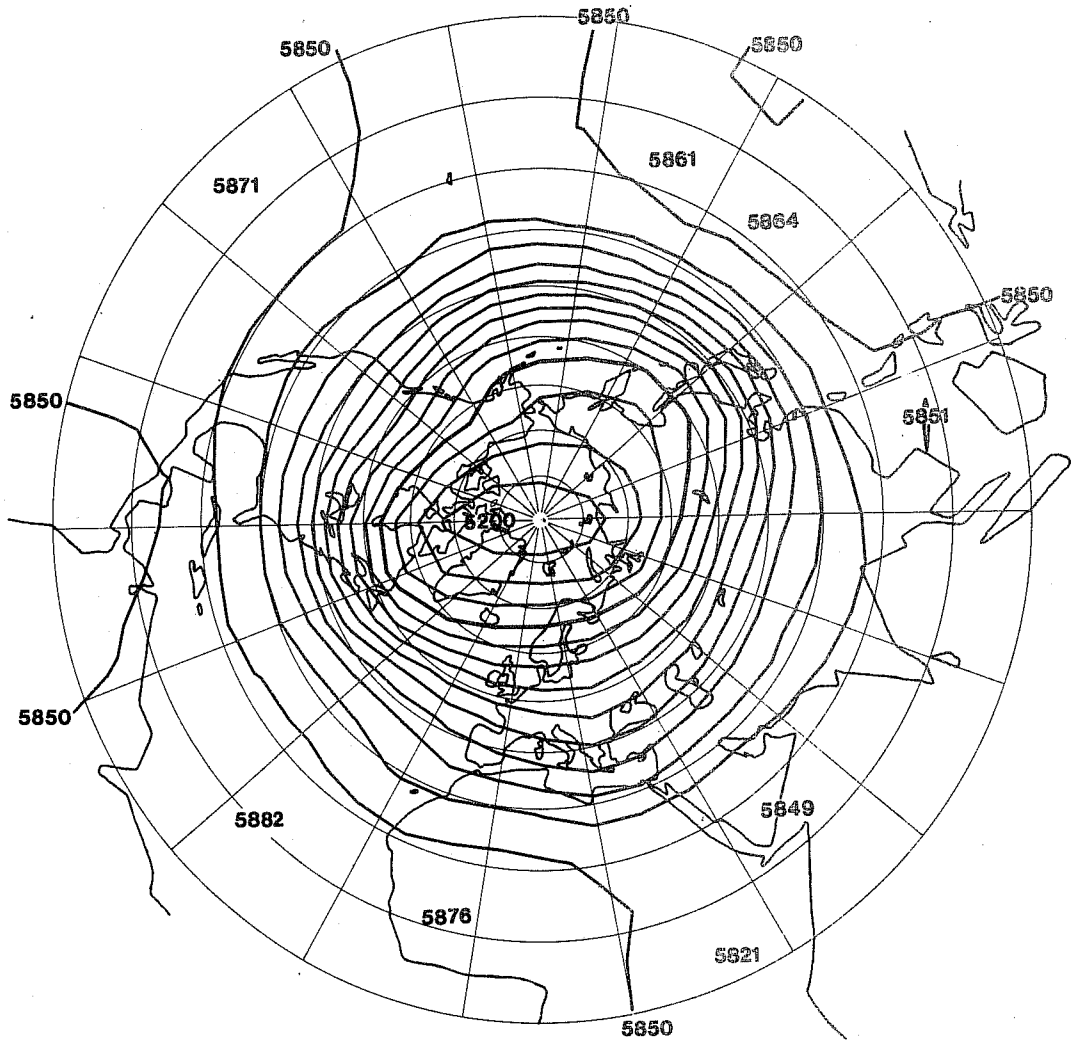

Figure 21 The mean field (temporal-wave number zero) of the height of the 500 mb level in gpm., spatial waves with wave numbers greater than 15 are filtered out.

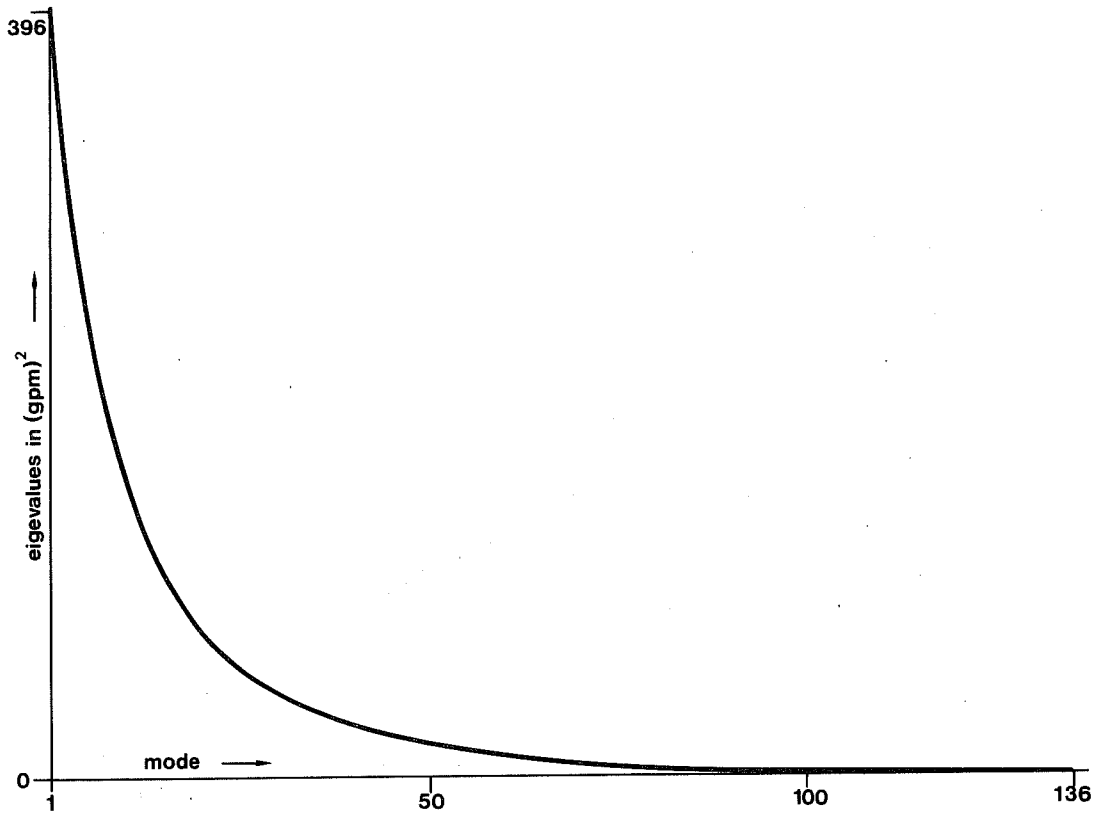

Figure 22 The eigenvalues of the covariance matrix of the deviation from the annual range of the height of the 500 mb surface of the Northern Hemisphere.

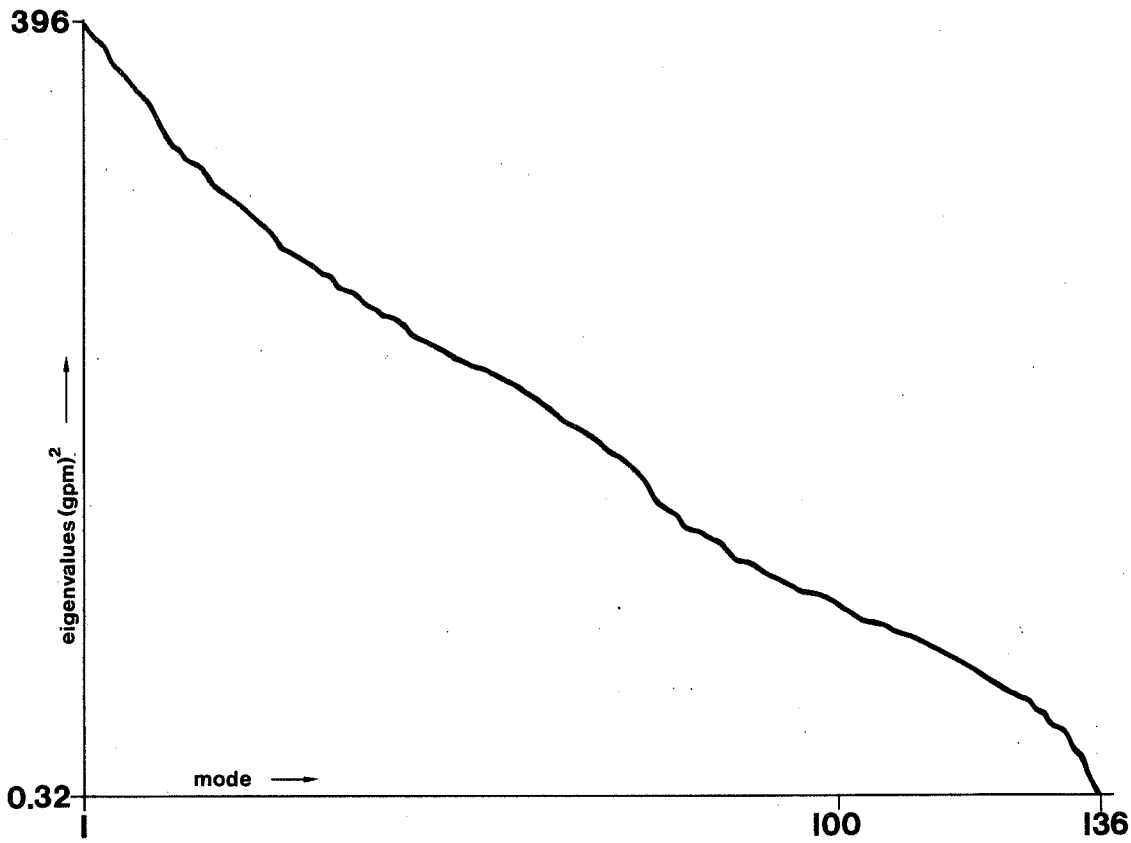

Figure 23 The eigenvalues of the covariance matrix of the deviation from the annual range of the height of the 500 mb surface of the Northern Hemisphere in a logarithmic scale.

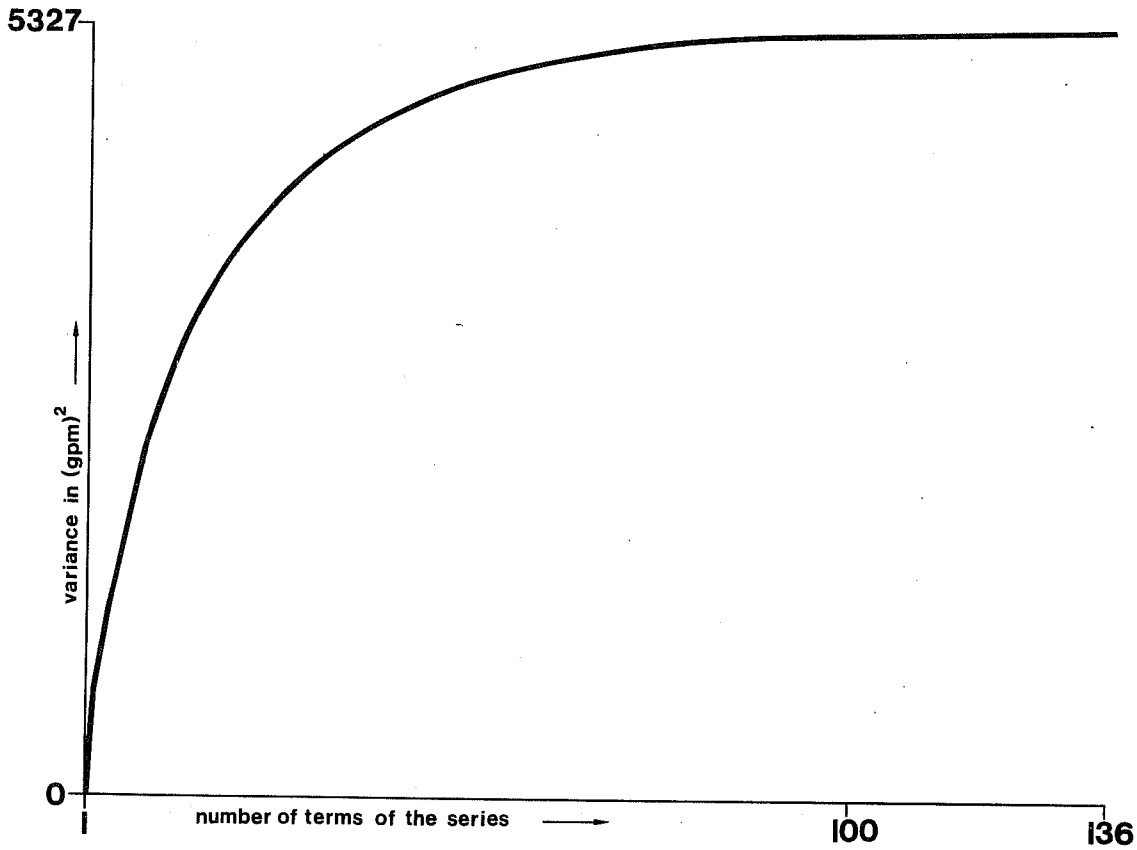

Figure 24 The variance of the partial series of eofs of the height of the 500 mb level of the Northern Hemisphere, without the part of the annual range.

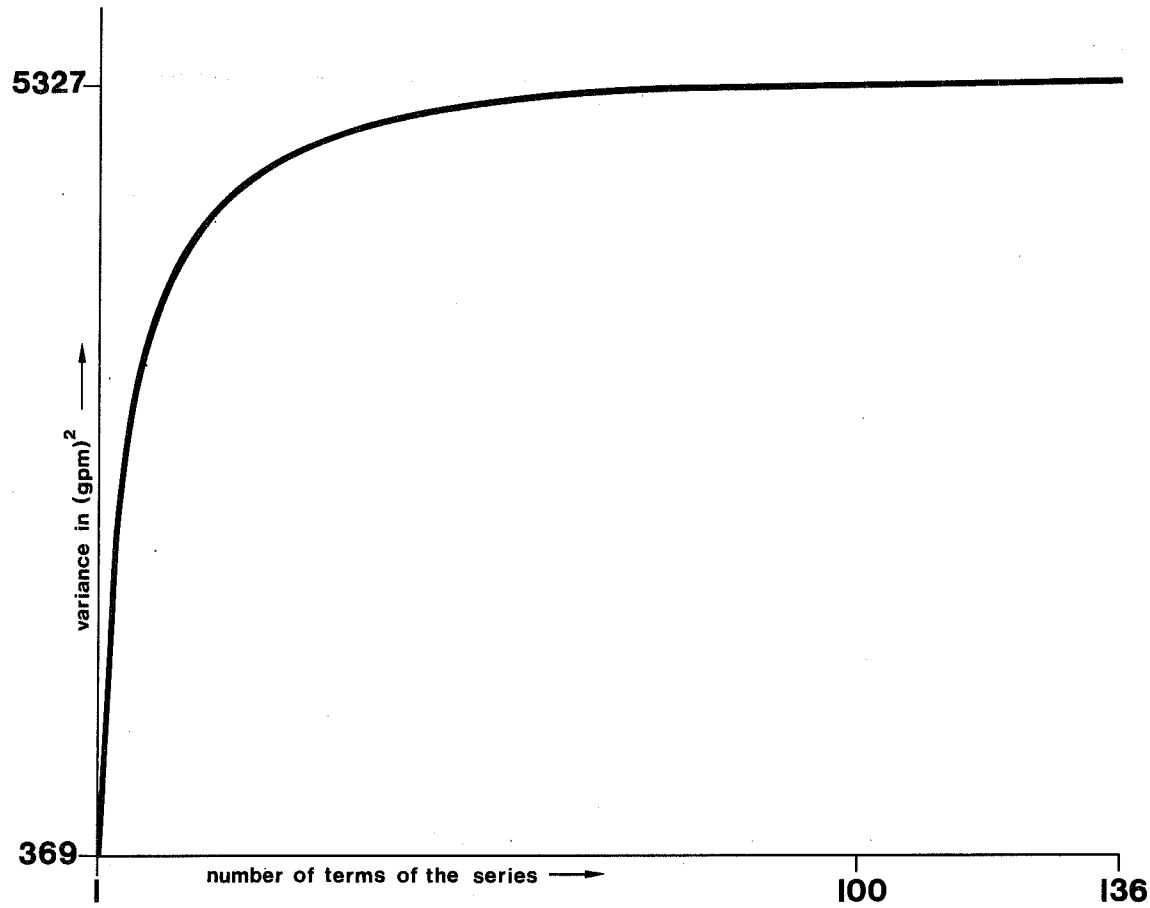

Figure 25 The variance of the partial series of eofs of the height of the 500 mb level of the Northern Hemisphere in a logarithmic scale.

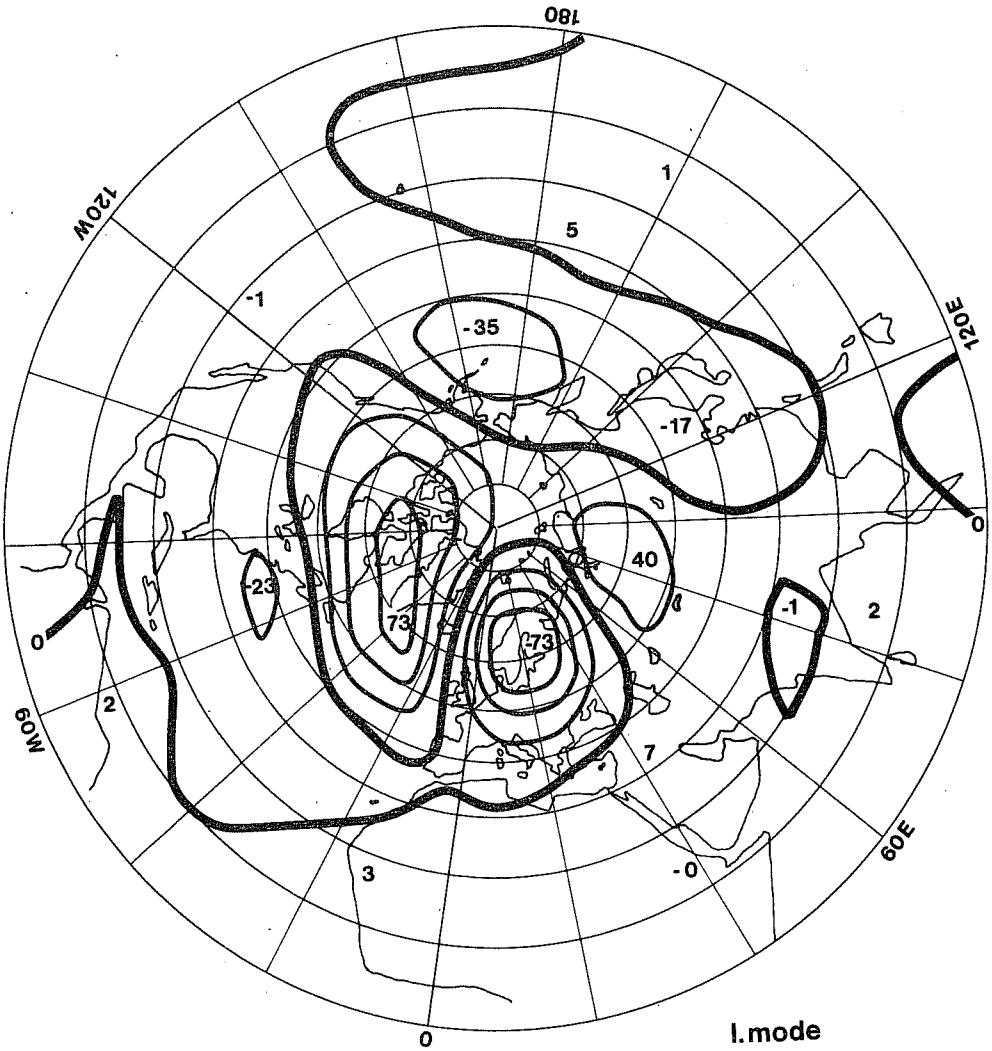

Figure 26 The first (most important) eof of the height of the 500 mb level in gpm, without the annual range

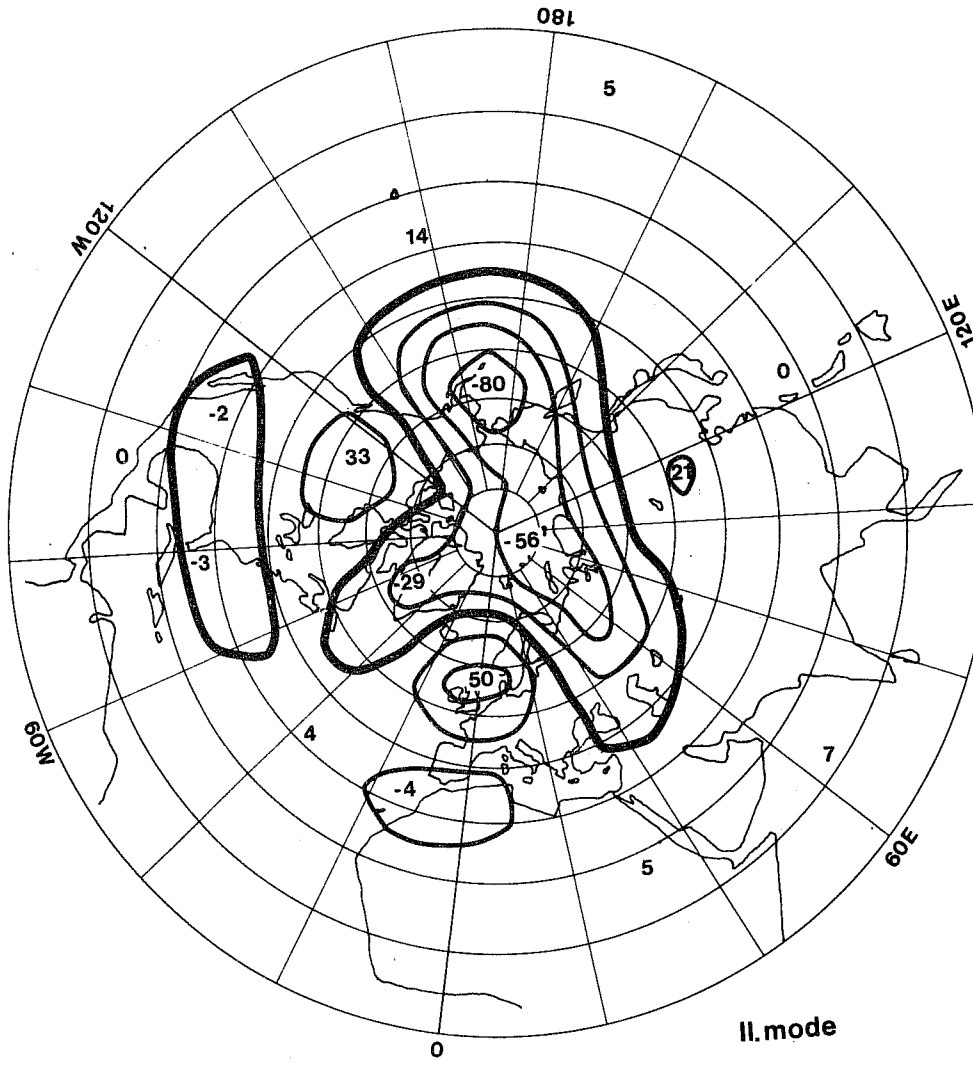

Figure 27 The second eof of the height of the 500 mb level in gpm.

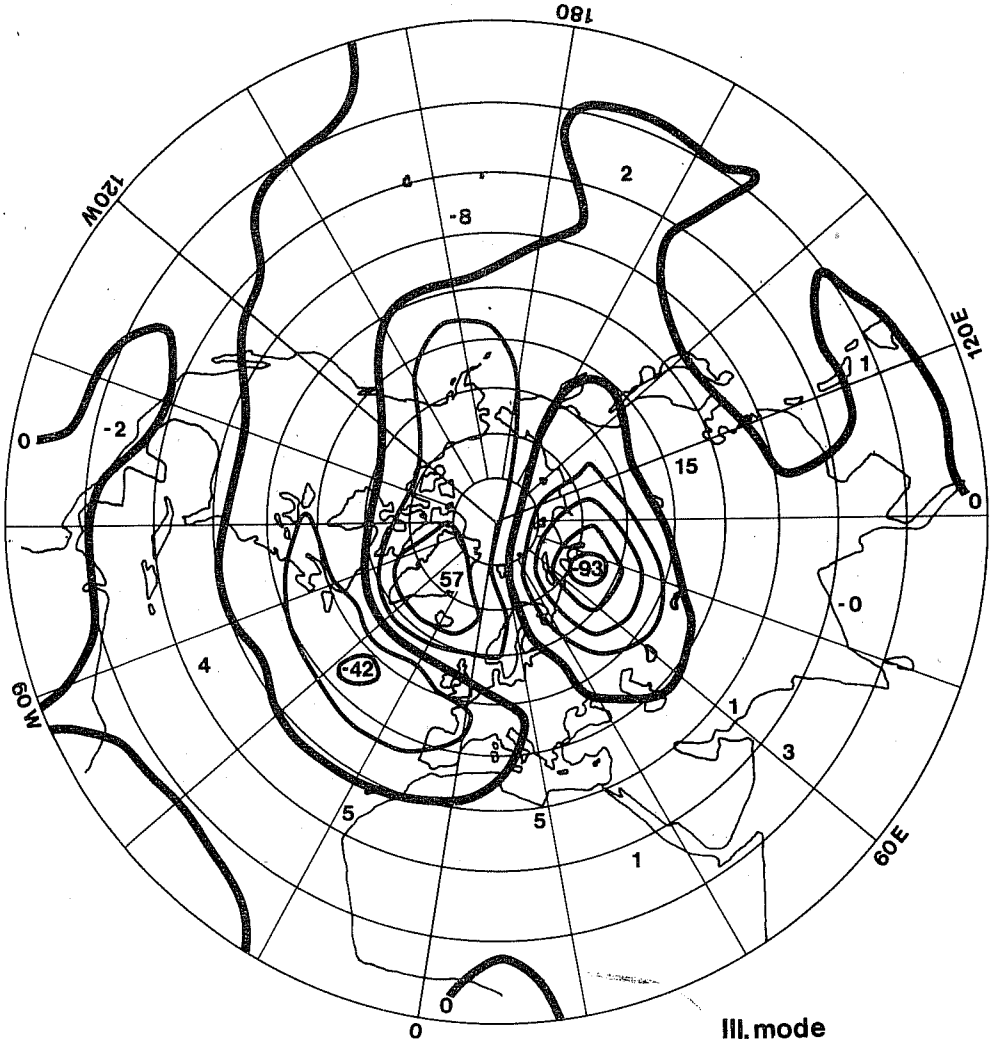

Figure 28 The third eof of the height of the 500 mb level in gpm.

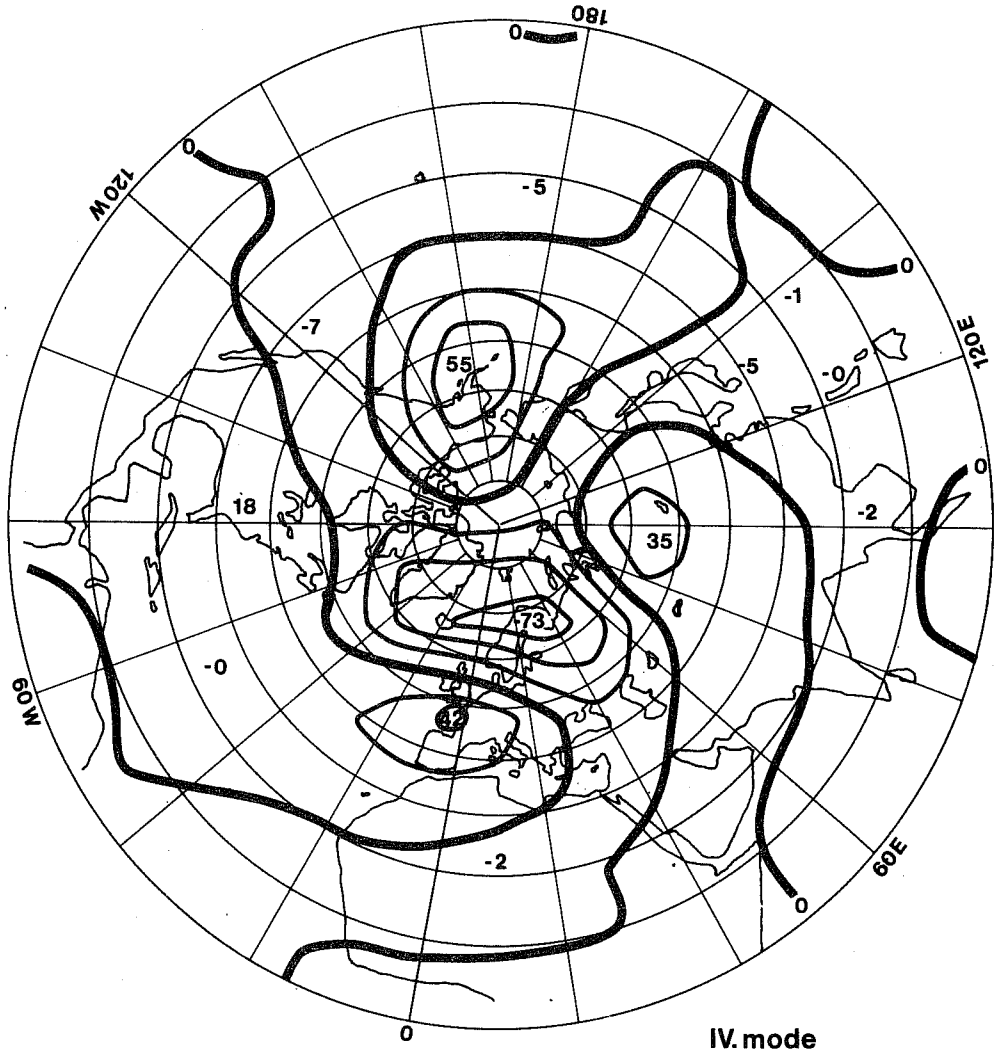

Figure 29 The fourth eof of the height of the 500 mb level in gpm.

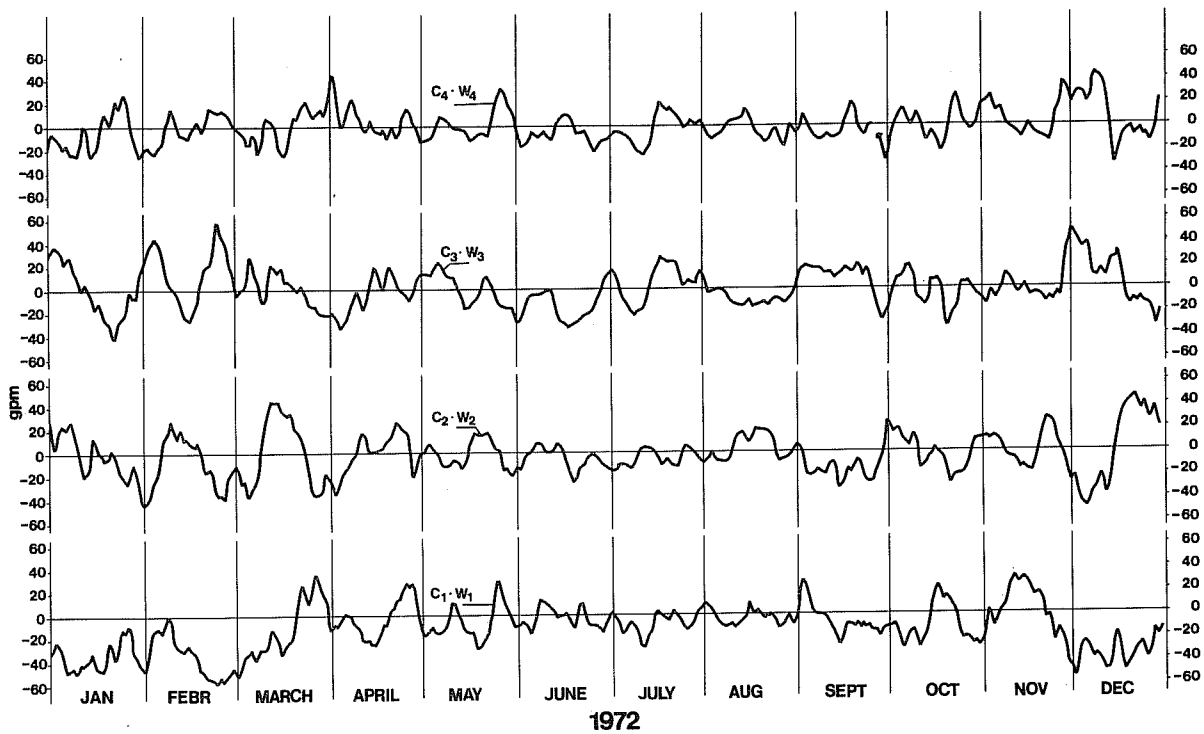

Figure 30 The variation of the first four most important time dependent coefficients of eofs of the height of the 500 mb level of the Northern Hemisphere in gpm, without the annual range.

The curve at the bottom represents the most important coefficient.